Editors' Suggestion

Routes for increasing endurance and retention in HfO_2-based resistive switching memories

Konstantin Z. Rushchanskii, Stefan Blügel, and Marjana Ležaić
Peter Grünberg Institut and Institute for Advanced Simulation, Forschungszentrum Jülich and JARA, 52425 Jülich, Germany

(Received 17 August 2018; published 27 November 2018)

We investigate metastable and thermodynamically stable phases that can be expected to occur in electroformed filaments in resistively switching hafnia, and discuss their relevance for the switching process. To this end, we conduct a study, based on density functional theory combined with an evolutionary algorithm determining the composition-dependent (meta)stable phases in HfO_x, focusing on the region $0 < x < 2$. We find that oxygen vacancies in hafnia tend to form regular patterns, which leads to periodic metastable structures featuring one-dimensional open channels, thus favoring ionic conductivity in the host material, i.e., oxygen migration. The band gap of such structures is systematically lowered with increasing oxygen deficiency, resulting in metallic behavior when oxygen migrates out of the channels. Moreover, we find that the solubility of oxygen in metallic Hf is very high, up to one oxygen per six metallic atoms, the concentration corresponding to a thermodynamically stable and ordered metallic compound, Hf_6O. Therefore, thick enough metallic capping of Hf could play the role of an active electrode for hosting oxygen which migrates out of HfO_2. In combination with reversible oxygen migration in predicted suboxide phases, this should lead to robust resistive memory cells with high endurance and long retention.

DOI: 10.1103/PhysRevMaterials.2.115002

I. INTRODUCTION

Recent interest in redox-based resistive random-access memories (ReRAM) is driven by their potential applications in future information technology as components of memory cells, active elements for multistate logics, neuromorphic computing, etc [1,2]. Those components are nonvolatile, fast, and scalable alternatives to the current flash-memory devices. The typical ReRAM device is based on a functional material (which is, in a very simple case, a binary oxide) placed between two metallic electrodes. The nanoscale size of the device allows for complex mixed conductivity, including the ionic, electronic, and quantum tunneling components, in materials which are typically good insulators in their bulk form [3]. Furthermore, during the forming step the material undergoes changes in highly nonequilibrium conditions that are a consequence of high temperatures arising from strong electric currents. Local heating in a strong electric field enables ionic transport, leading to strong deviation of the stoichiometry in the active area of the device, and, possibly, to formation of multiple phases and/or extended defects. Moreover, local high-temperature conditions facilitate internal redox reactions, which could appear in the bulk of the functional material, as well as in the area of the interface with conductive electrodes. Therefore, one can distinguish two fundamentally different mechanisms: (*i*) operability of the device is driven by redox processes on the electrode metal in the so-called electrochemical metallization memory (ECM); (*ii*) the oxide layer is serving as a (nano)electrolyte in the case of valence change memories (VCMs). In reality one can expect a mixture of both mechanisms [4,5].

Active areas of VCMs with significantly modified conductivity take the shape of extended filaments. The structure, composition, and control of the formation processes that lead to well-defined filaments are some of the important unknowns of the field. Understanding the microscopic mechanisms of processes involved in forming and switching is not an easy task, due to the small size of the active area, typically of the order of a few tens of nanometers. Standard x-ray based experimental methods to study the filaments, such as photoelectron spectroscopy (XPS) and absorption spectroscopy (XAS), typically face problems due to complex preparation of samples, difficulties in locating the filament position, and limited spatial resolution, which leads to measurements averaged over the whole sample. Transmission electron microscopy (TEM) is further complicated by the necessity of preparing very thin samples containing lateral cuts through the filament in required geometries. With a new experimental method, the scalpel scanning probe microscopy [6], one gains the ability to locate the filaments and to measure electric properties of individual active areas [7]. However, the structure of the filament is not accessible by this approach and, therefore, our understanding of it is still lacking.

Due to the aforementioned difficulties, the details of the mechanisms driving the switching are still under debate, despite the fact that ReRAM devices are intensively investigated and already commercialized. So far, several important points are commonly accepted [1]. It is now well-established that the resistance switching in metal oxide memristors is mediated by oxygen migration [8,9], resulting in formation of the conductive filaments, while the details of the filament formation as well as the type of switching (bipolar vs unipolar) depend on the nature of electrodes [10] and on the interfacial metal-oxide interactions [5].

Numerous materials have so far been investigated and shown to posses the resistive switching properties. For example, a lot of work was dedicated to Ti-containing oxides [11–16], but also many other transition-metal oxides that show similar behavior (see Ref. [1] and references therein). In particular, for TiO_2-based ReRAM it was observed [17] that the

switching occurs by the formation of the suboxide crystalline Ti_4O_7 Magnéli phase (conductive above 149 K [18]) in the filament. Magnéli phases, with a generic formula Ti_nO_{2n-1} ($4 \leqslant n \leqslant 10$) [19]) are easily obtained from the rutile form of TiO_2 [20]. However, when starting from its anatase form, Ti_4O_7 is only an intermediate product during the reduction, while the materials are finally reduced to Ti_2O_3 and Ti_3O_5 in a prolonged reduction time [21]. Therefore, the formation of the conductive filament in TiO_2 can be seen as a local reduction of the stoichiometric oxide to one of its metastable forms [22,23] from the Magnéli series. During the forming cycle, metastable suboxide phases can thus be formed by quenching the host material under nonequilibrium conditions, possibly resulting in the desired switching properties.

In this paper, we keep in mind both the example of TiO_2 and the fact that the metastable phases have not, to our knowledge, been confirmed so far in the filaments of other investigated resistively switching oxides, and we conduct a computational study in order to shed light onto the filament structure and its relation to the (electronic and ionic) conductance as well as the switching mechanism. Since the phase space to be sampled grows rapidly with the number of atoms, we focus here on a binary compound. Our choice is hafnia, HfO_2, that is in use as a gate oxide and thus is well integrated in the processing of the semiconductor industry, and for which a significant experimental background is available.

Previously, it was theoretically shown [24–26] that a chain of vacancies in the insulating hafnia host results in a conductive channel. The conductivity can be destroyed by recombination with oxygen, which restores the insulating state. Recent first-principles simulations were performed to identify an optimal HfO_x stoichiometry, where $1.5 < x < 1.75$, and the critical radius for the nucleation and growth of a stable conductive Hf-rich cluster [27]. It was further predicted theoretically that the stability of oxygen vacancies in monoclinic HfO_2 is enhanced at grain boundaries as compared to the bulk crystal, which helps the formation of the conductive filaments [28]. This prediction is well in line with the experimental observations of the enhanced oxygen deficiency near extended defects in polycrystalline HfO_x films [5,29]. Structure and electronic properties of various hafnium suboxides HfO_x were studied by means of *ab initio* simulations in a wide range of concentrations. In Ref. [30] a cluster expansion method was used for a ground state analysis and for the calculation of the phase diagram for the hexagonal close packed (hcp, α phase) octahedral-interstitial solid solution system αHfO_x.

An investigation of the full range of Hf-O binary compounds [31] by means of an evolutionary algorithm [32–34], which was devoted to a search for new phases stable at high pressures in order to characterize their mechanical properties, shows that $Pnnm$-Hf_2O, $Imm2$-Hf_5O_2, $P\bar{3}1m$-Hf_2O, and $P\bar{4}m2$-Hf_2O_3 high-pressure phases become metastable at ambient pressure. $P\bar{4}m2$-Hf_2O_3 structure was also predicted in Ref. [35], where first-principles DFT calculations were employed to search for stable metallic oxygen-deficient hafnium and zirconium oxides, which may be reachable at normal conditions from monoclinic hafnia and zirconia with assistance of an applied electric field. It should be noted, however, that the mentioned theoretical structural studies [30,31,35] were performed with the generalized gradient approximation for exchange and correlation energies [36]. This approach neglects possibly strong correlation effects within the Hf d shell, which may affect the Hf-O interaction and bonding [25].

With the goal of investigating the filament's structure and its role in the resistive switching, we investigate possible crystalline structures of the those phases which may form the filaments with electronic and/or ionic conductance, and analyze their importance for the reversible resistive switching mechanisms in HfO_2. We apply state-of-the-art theoretical methods, combining density functional theory (DFT) with an evolutionary compositional and structural algorithm, as used in Ref. [31], to collect information about the crystalline structure of possible metastable states in HfO_2 off-stoichiometric binary oxides, which could be formed and consequently quenched in an electroforming process by programming the memory cell. Since strong correlation effects within the d shell of Hf have the potential to alter the stability of individual phases, we take them into account in a DFT+U approach [37].

We obtain a composition diagram, which contains new metastable crystalline phases with one-dimensional open channels, which can accommodate oxygen in different amounts. The oxygen concentration in these channels can be easily changed, which goes along with a changing electrical resistivity. The prediction of new crystal phases in substoichiometric HfO_2 with one-dimensional channels and their interrelation with ionic and electrical conduction properties shed new light on the microscopic mechanism of reversible resistive switching, and can help develop strategies for increasing the endurance and retention of hafnia-based ReRAM devices, assuming that these metastable phases emerge as nanophases during the formation of the filament under nonequilibrium conditions.

II. COMPUTATIONAL DETAILS

To study structures at various compositions in Hf-O binary solid solutions we utilized an evolutionary algorithm as implemented in the USPEX code [32–34,38]. The method uses series of variation operators to produce offspring structures based on the previous generations: the heredity operator, which defines and conserves spatially coherent pieces of the parent structures to produce the next generation candidate structures; softmutation, which uses low-energy phonon mode eigenvectors to produce new optimized structures; lattice mutation, which incorporates the ideas of metadynamics [39], where new structures are found by building up cell distortions of some known structures; and transmutation, when randomly selected atoms are transmuted into other chemical species. Random structures with random space-group (SG) symmetry were used for the initial generation. Subsequent generations were obtained by variation operators including heredity (with the ratio 40% of all structures), lattice mutation (20%), random structures (20%), and transmutation (20%). Initially, we allowed up to 48 atoms in the calculation cell in the whole composition range Hf-O and started from 60 random structures. Subsequently, focusing on the range of compositions HfO-HfO_2, we performed additional calculations, allowing for up to 96 atoms per calculation cell, in order to obtain a better sampling of the near suboxide region of HfO_2. In this region we used the seeds technique as implemented in the USPEX code, where the seed structures were based on our previous results obtained with maximum 48 atoms per cell.

Ground state properties and structure relaxations in Hf-O systems during the evolutionary algorithm runs were obtained with the Vienna Ab initio Simulation Package (VASP) [40–42], utilizing projector-augmented wave potentials [43] with the following valence-electron configurations: $5s^2 5p^6 6s^0 5d^4 5f^0$ (with $4f^{14}$ electrons frozen in the core) for Hf and $2s^2 2p^4$ for O. In total, we performed *ab initio* calculations for about 5500 different structures with varying content of oxygen. We used the Perdew-Burke-Ernzerhof exchange and correlation functional revised for solids (PBEsol) [44], with DFT+U correction on the Hf d shell choosing $U = 7$ eV and $J = 1$ eV, as in Ref. [25]. In order to check whether the calculated composition diagram depends on the particular choice of the Hubbard U, we recalculated the diagram with a large set of U parameters, $0 \leqslant U_{\text{eff}} \leqslant 6$ eV (where $U_{\text{eff}} = U - J$) [45]. Although the absolute numbers, as expected, do vary from case to case, the most important results presented in this paper remain valid (see the discussion of the results for details). A plane-wave energy cutoff of 600 eV was used for all calculations. Uniform Γ-centered k-point meshes with resolution $2\pi \times 0.03$ Å^{-1} were used to sample the Brillouin zone. To confirm the dynamical stability of relevant phases, we calculated the phonon dispersions by means of the finite-displacement method employing the PHON code [46]. Migration barriers for ionic diffusion were calculated with a standard nudged elastic band (NEB) method [47] as implemented in the USPEX code.

III. RESULTS AND DISCUSSIONS

A. Energetics and structure of metastable HfO_x phases

The stability of various phases of a compound (in our case, Hf-O binary compound) can be presented in the form of a so-called *convex hull* [38] or, alternatively, in a *fitness plot* [32]. In the former form, the enthalpy of formation (i.e., the cohesive energy of a HfO_x phase relative to the composition-weighted average cohesive energies of pure Hf and O in their stable forms) is plotted, versus the atomic ratio x of oxygen to hafnium. A newly determined phase is considered thermodynamically stable if its formation enthalpy is lower than that of any other structure, or any combination of structures that gives the proper composition. The name "convex hull" refers to the line connecting thermodynamically stable compounds found in the calculation for varying x. In the latter form (fitness plot), δH, the formation enthalpy of HfO_x phases with respect to the convex hull lines (also referred to as the "fitness" of these phases), is plotted versus x. Thermodynamically stable phases have $\delta H = 0$, whereas for all metastable ones $\delta H > 0$. This presentation is more convenient for evaluating metastable phases, since δH is, in a sense, the figure of merit showing how probable the formation of the corresponding metastable compound is.

Figure 1 summarizes our *ab initio* calculations in the form of a fitness plot, showing the calculated structures in the lowest range of $\delta H < 0.2$ eV/atom. The calculations yield pure metallic Hf in its hexagonal close packed (hcp) $P6_3/mmc$ crystalline structure and oxygen in its molecular form, along with several thermodynamically stable compounds. For oxidized Hf, we find HfO_2 with its monoclinic $P2_1/c$ crystal

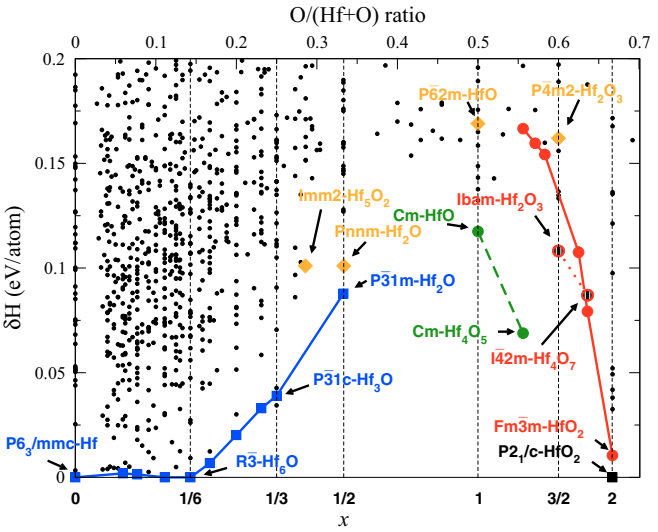

FIG. 1. Composition diagram in the Hf-O system. Energies are given in eV per atom as a distance δH from the convex hull to the metastable phase. Hexagonal Hf and molecular O_2 form boundaries; hexagonal Hf_6O and monoclinic HfO_2 are thermodynamically stable compounds. The blue line indicates a boundary of phases with hexagonal structure, where oxygen atoms occupy vacant octahedral positions in a hexagonal close packed structure of metallic Hf. The red line indicates a boundary of suboxide phases with fluorite structure. The dotted red line defines region of fluorite structures with ordered one-dimensional chains of oxygen vacancies. The dashed green line indicates crossover between hexagonal and fluorite structures (see text for discussions). Diamonds are structures obtained in Ref. [31]. Lines are given as a guides for the eyes. Black dots are the relaxed phases of trial structures at the end of the evolutionary algorithm search. The lower scale shows the atomic ratio of oxygen to hafnium (i.e., the concentration of O, x, in the compounds HfO_x), whereas the upper one defines the atomic percent of oxygen in the compounds. In the plotted energy range no metastable structures were found for concentrations above $x \geqslant 2$.

structure as the most stable compound, in agreement with experiment [48]. In addition, along the line connecting Hf-HfO_2 we find another stable compound, Hf_6O with SG $R\bar{3}$, also in agreement with experiment [49] as well as with previous theoretical works [30,31]. However, for the purpose of getting microscopic insight into resistive switching processes, it is important to analyze the crystal structure not only of the thermodynamically stable compounds, but also of the metastable compounds with (possibly strong) deviation from stoichiometry in the vicinity of the stable compounds.

Based on the results of our simulation, the composition diagram of the Hf-O system can be divided into four regions, as shown in Fig. 1: (*i*) The vicinity of pure Hf, where the hcp structure is preserved and the extra content of oxygen is distributed among the interstitial positions octahedrally coordinated by Hf atoms. This region extends up to the concentration $x = 1/2$, which corresponds to the metastable crystalline compound Hf_2O. Crystal structures are characterized by different space groups, depending on the ordering of the oxygen interstitials in the hcp matrix. The phases of this region are shown in blue color. (*ii*) A crossover region is found in the narrow range of $1 \leqslant x \leqslant 1.25$, where monoclinic

phases of HfO_x with Cm symmetry are shown in green color. (iii) The vicinity of HfO_2 with suboxide stoichiometry $(1.25 \leqslant x \leqslant 2)$, shown in red color. Compounds in this region originate from the cubic phase of HfO_2 with a fluorite-type crystal structure. (iv) A superoxide region for $x > 2$ and above towards pure oxygen. The formation enthalpy differences, δH, for compounds in this region are much higher than for the HfO_2 suboxide regions, which, we believe, excludes possible quenching of these structures during the electroforming processes. We will, therefore, in the following focus only on the previously mentioned three regions and discuss their relevance for the resistive switching in detail.

Region (i). This region is as important for the resistive switching as the suboxide regions (ii) and (iii), because the processes in which oxygen diffuses into the metallic electrodes and the subsequent formation of an interface layer between the oxide and electrodes are both important for the durability and reproducibility of cycle-to-cycle parameters, as well as for the aging with subsequent device failure [9]. Recently, it was shown [5,7,50] that introducing an oxygen scavenger layer results in a better device performance by facilitating the formation of conducting filaments, and reduces the dependence of device's behavior on the microstructure in its "on" state [51].

We find that metallic Hf can easily absorb oxygen up to one oxygen atom per six Hf, when ordered Hf_6O is formed. Namely, in the range Hf-Hf_6O, metastable compounds almost follow the convex hull line, $\delta H = 0$. Moreover, many structures in this region are characterized with low δH, indicating a strong degeneracy of the crystal structures and, correspondingly, high configuration entropy. This result shows that the Hf electrode acts as a reservoir for oxygen which migrates out of the oxide region during electroforming and/or switching cycles.

It is noteworthy that the most stable structures of this region are those where oxygen interstitials form one-dimensional chains along the hexagonal c axis, with alternating occupation (i.e., only every second void along the c axis is occupied, leading to a structure with distinct oxygen-rich layers). Varying the oxygen concentration leads to a variation of the density of such chains in the plane perpendicular to the c axis, but the chains are present already for the lowest calculated concentration $Hf_{16}O$ and are also seen in $Hf_{12}O$, $Hf_{10}O$, and Hf_8O. Once Hf_6O is reached, the formation of one-dimensional chains along the hexagonal axis is not favored anymore, the interstitial positions of the hcp Hf lattice contain oxygen in every hexagonal plane [see Fig. 2(a)], and the structure possesses $R\bar{3}$ symmetry. Note that this result stands in full agreement with the experimental observation of Ref. [49], where the structure of the hypostoichiometric composition $HfO_{1/6-}$ was found to possess $R\bar{3}$ symmetry for the oxygen concentration of 13.4%. In our calculations, the highest oxygen concentration in the structures forming one-dimensional O chains is 11.1% for Hf_8O. Furthermore, when the content of oxygen in experiment is increased to 15.8%, superstructures with $P\bar{3}1c$ symmetry are formed [49]. This observation is also in agreement with our calculations (see Hf_3O in Fig. 1(b).

Our calculations in region (i) agree with previous theoretical works [30,31], where the generalized gradient approximation PBE [36] was used (without taking into account strong exchange-correlation effects on Hf d orbitals).

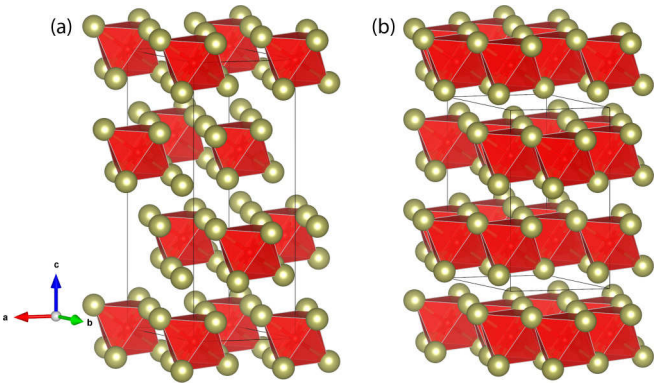

FIG. 2. Crystal structures of (a) $R\bar{3}$-Hf_6O and (b) $P\bar{3}1c$-Hf_3O, showing the preferred occupation with oxygen in vacant octahedrally coordinated positions (depicted by the red octahedra) in hcp Hf host (yellow spheres).

Region (ii). As follows from our results, the solubility of oxygen in the hcp structure is limited to ~30 mol %. At higher concentrations, we find that the metallic Hf oxidizes and probably forms Cm-Hf_4O_5, which has a lower fitness energy, δH, than the aforementioned Hf_2O (see the structures shown in green color in Fig. 1). This "crossover" region found in our simulation is different from the results obtained in previous studies. For example, in Ref. [30] it was assumed that oxygen occupies interstitial octahedral positions of the hcp structure of metallic Hf up to the concentration $x = 1.0$ (i.e., HfO). However, as it can easily be seen by extrapolating the fitness energies of hcp-like structures in region (i) (blue solid line in Fig. 1) the resulting structures have higher energies than the ones obtained in our work. Furthermore, the $P\bar{6}2m$-HfO structure, obtained in Ref. [31] (see orange diamonds in Fig. 1), is also higher than the monoclinic Cm-HfO structure, identified in our calculation.

The low-δH compounds of the crossover region are characterized by the same structural frame, based on the monoclinic Cm-HfO, which is different both from the hcp and from the monoclinic hafnia structure (see Fig. 3). Namely, Cm-HfO could be seen as consisting of layered building blocks, connected by covalent bridges. From the point of view of the resistive switching, the most important feature of this structure is the presence of one-dimensional vacant channels, which can be filled up by extra atoms of oxygen as the O concentration rises, resulting ultimately in Cm-Hf_4O_5 where all previously vacant positions of the chain are filled [compare structures in Figs. 3(a) and 3(b); their symmetry, composition and structural parameters are given in Tables I and II]. The two endpoints of the crossover region, i.e., Cm-HfO with ordered vacant channels and Cm-Hf_4O_5 with the channels completely filled by oxygen, are connected by the green dashed line in Fig. 1. Between these two points, compounds with different filling of the channels (depending on particular O concentration) can exist. The electrical conductivity of these structures depends on the channel filling: Cm-HfO is a metal, Cm-Hf_4O_5 is a band insulator, while structures with incomplete channel-filling show varying band-gap widths (or metallic behavior).

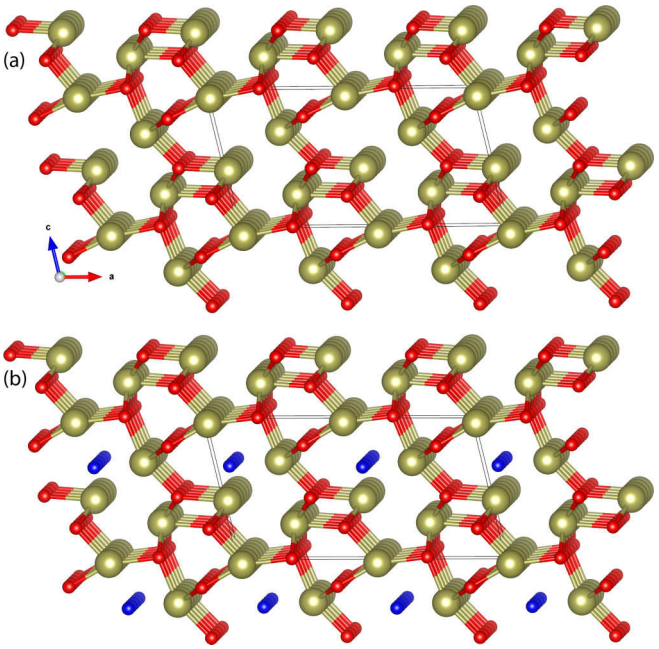

FIG. 3. Crystal structures of the monoclinic phases of (a) Cm-HfO and (b) Cm-Hf_4O_5, in the crossover region of the Hf-O composition diagram. Both structures share the same structural frame; however, Cm-Hf_4O_5 contains extra oxygen (shown by small blue spheres), which occupies the vacant positions present in Cm-HfO structure, forming one-dimensional chains. Hf atoms are depicted with yellow spheres. Oxygen atoms which are the constituents of the structural frame are shown as red spheres.

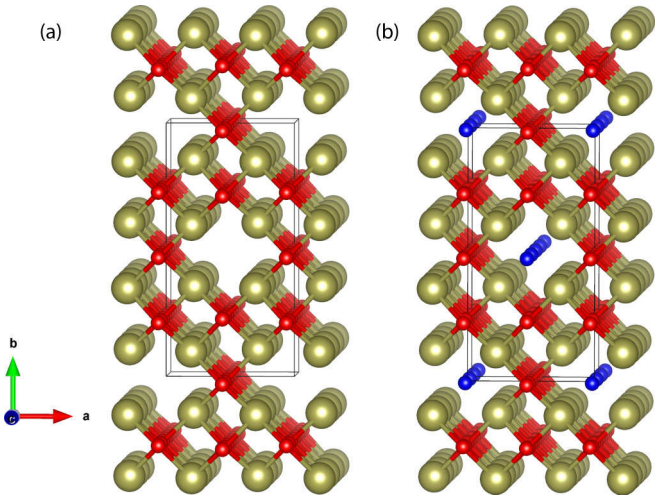

FIG. 4. Crystal structures of (pseudo)tetragonal fluorite-like phases of (a) $Ibam$-Hf_2O_3 and (b) $I\bar{4}2m$-Hf_4O_7 in the suboxide region of hafnia. In metallic $Ibam$-Hf_2O_3 one-dimensional chains of oxygen vacancies are clearly seen. These chains are partially filled up by oxygen (shown by small blue spheres) in Hf_4O_7, resulting in an insulating state. The ordered $Ibam$-Hf_2O_3 phase is clearly split off from the rest of the structures of region (iii) (see the solid red line in Fig. 1), indicating the natural preference of oxygen vacancies to form one-dimensional chains.

Here we should note that in Ref. [25] the conductive path in HfO_2 ReRAM was attributed to negatively charged oxygen vacancy chains, which are responsible for the formation of partially occupied defect states in the electronic density of states. It was shown that the electroforming process is initiated by a supply of neutral oxygen Frenkel defect pairs, and the accumulation of the oxygen vacancies results in the formation of local metallic suboxide phases, HfO_x, which remain conductive even as ultranarrow filaments in the insulating matrix. Therefore, our findings are in full agreement with this view on the conductivity of filaments, adding the knowledge that accumulation of the oxygen vacancies is a natural process, which results in the formation of vacancy chains.

The described properties of the compounds in this region could facilitate the migration of oxygen from the inner part of HfO_x films to the electrodes, leading to resistive switching behavior for strongly oxygen-deficient hafnia. However, it is more probable that the resistive switching is enabled by the structural properties of the compounds from region (iii), i.e., from the near-suboxide region of HfO_2, which is, in our calculation as well as empirically, the most stable compound of the composition diagram.

Region (iii). Interestingly, aside from a different structural frame characterizing the compounds of this region, the functional features we observed in region (ii) are also present here. We find in this region a sequence of crystalline phases derived from cubic HfO_2 with fluorite-like structure, where oxygen vacancies form different patterns (see the solid red line in Fig. 1). The presence of oxygen vacancies embedded into the cubic HfO_2 frame leads to a variety of structures, which (on average) could be seen as a tetragonal phase in experiments [52]. In all the metastable structures of this region, Hf atoms are at the positions which correspond to the cubic HfO_2 phase. Therefore, these structures can easily be realized by only extracting oxygen from the stoichiometric host during the electroforming process.

When moving into the HfO_2 suboxides, we find the $Ibam$-Hf_2O_3 (or, in the corresponding suboxide notation, $HfO_{1.5}$) structure, as the lowest-δH phase for $x = 1.5$. In Fig. 1, this phase is connected by the dashed red line to Hf_4O_7 ($HfO_{1.75}$). Importantly, these two structures are related to each other in the same way in which the two lowest-δH structures of region (ii) are related. Namely, in the crystal lattice of $Ibam$-Hf_2O_3, oxygen vacancies are ordered into periodic, one-dimensional channels incorporated into a fluorite-like structure (see Fig. 4 and Table II). When the channels are half filled with oxygen, which is equidistantly distributed along the channel, the resulting structure is that of Hf_4O_7. The conductivity again depends on the channel filling: the structure with partially filled channels (Hf_4O_7) is a band insulator, while the one with empty channels ($Ibam$-Hf_2O_3) is metallic (see Table I). For varying oxygen concentration between these two structures (i.e., for varying channel filling), we obtain varying widths of the band gap (or metallic behavior for low filling). Thus, although in regions (ii) and (iii) the structural frame and the associated lattice symmetry are different, ordered one-dimensional empty channels exist in the lowest-δH metallic structures of both regions, allowing for the possibility of easy oxygen migration and resistive switching.

TABLE I. Short summary of structural and electronic properties of HfO_x phases.

Phase	Composition	SG No.	SG	Fitness (δH) (eV/atom)	Band gap (eV)
Hf_6O	$HfO_{0.16}$	148	$R\bar{3}$	stable	metal
HfO	HfO_1	8	Cm	0.114	metal
Hf_4O_5	$HfO_{1.25}$	8	Cm	0.068	0.28
Hf_2O_3	$HfO_{1.5}$	72	$Ibam$	0.107	metal
Hf_4O_7	$HfO_{1.75}$	121	$I\bar{4}2m$	0.079	0.54
HfO_2	HfO_2	14	$P2_1/c$	stable	4.43

In contrast to region (i), where DFT+U results coincide with previously reported PBE studies [30,31], sequences of the low-energy phases in region (iii) differ from the ones reported in Ref. [31]. For example, we find that the $P\bar{4}m2$-Hf_2O_3 phase reported in Refs. [31,35] is situated significantly higher than the phase $Ibam$-Hf_2O_3 with ordered one-dimensional channels (see Fig. 1) reported here. In Ref. [45] we address the question of the choice of exchange and correlation functional, choosing the PZ [53], PBE, and PBEsol functionals (i.e., using both local density and generalized gradient approximations) in combination with different U_{eff} values up to 6 eV, as well as the hybrid B3LYP [54,55] and Heyd-Scuseria-Ernzerhof (HSE) [56,57] functionals, and investigate in more detail the influence different approaches have on the composition diagrams in Hf-O, Zr-O, and Y-O systems. Here we note that the relative position of $Ibam$-Hf_2O_3 and $P\bar{4}m2$-Hf_2O_3 strongly depends on the choice of U. However, for all reasonable values [25] of U_{eff} above ∼3 eV with the PBE functional (and ∼4 eV for PBEsol), the $Ibam$-Hf_2O_3 phase has a lower energy than the $P\bar{4}m2$-Hf_2O_3 one. For $U_{\text{eff}} \leqslant 3$ eV (or $U_{\text{eff}} \leqslant 4$ eV for PBEsol) including the calculations performed with $U_{\text{eff}} = 0$ eV, $P\bar{4}m2$-Hf_2O_3 has the lowest energy, as reported previously [30,31]. The position of the Cm-HfO and Cm-Hf_4O_5 phases from region (ii) is less sensitive to the choice of U, and they remain the lowest-energy structures of this region in the range of U_{eff} from 0 up to 6 eV (i.e., the phase Cm-HfO has always a lower energy than the previously reported $P\bar{6}2m$-HfO phase [31]).

B. Functionality with respect to forming and switching

It should be emphasized that the structures we are discussing here are actual metastable phases (aside from the two thermodynamically stable phases of the binary compound that were also found), i.e., they show dynamic stability and are likely to be quenched during the electroforming process as the most stable phases for a given stoichiometry, without decomposing to thermodynamically stable compounds. Even the phases that contain lattices of completely empty one-dimensional channels show stable phonon structures (see Fig. 5 for the phonon spectrum of $Ibam$-Hf_2O_3). One should, however, bear in mind that in a real sample the channels are most probably not equally filled, which makes it experimentally difficult to identify the crystal symmetry and yields an overall picture of random vacancy distributions already in a single crystal, but even more so in polycrystalline samples.

TABLE II. Structural properties of selected phases in the Hf-O system.

Compound	Space group	Lattice constant (Å)	Wyckoff position	x	y	z
HfO	Cm (No. 8)	$a = 11.822$	Hf1 2a	0.25584	0.0	0.71509
		$b = 3.381$	Hf2 2a	0.76940	0.0	0.26785
		$c = 6.283$	Hf3 2a	0.03806	0.0	−0.02261
		$\beta = 103.08$	Hf4 2a	0.53579	0.0	0.44462
			O1 2a	−0.04495	0.0	0.25389
			O2 2a	0.23073	0.0	0.04559
			O3 2a	0.86218	0.0	0.83056
			O4 2a	0.35296	0.0	0.46527
Hf_4O_5	Cm (No. 8)	$a = 11.921$	Hf1 2a	0.25813	0.0	0.71763
		$b = 3.315$	Hf2 2a	0.76477	0.0	0.2781
		$c = 6.436$	Hf3 2a	0.03815	0.0	0.0006
		$\beta = 103.42$	Hf4 2a	0.53579	0.0	0.44462
			O1 2a	0.94715	0.0	0.25282
			O2 2a	0.2289	0.0	0.04275
			O3 2a	0.86765	0.0	0.83649
			O4 2a	0.35258	0.0	0.47193
			O5 2a	0.06918	0.0	0.68136
Hf_2O_3	$Ibam$ (No. 72)	$a = 5.055$	Hf 8j	0.25126	0.62524	0.0
		$b = 9.998$	O1 4b	0.5	0.0	0.25
		$c = 5.160$	O2 8g	0.0	0.2425	0.25
Hf_4O_7	$I\bar{4}2m$ (No. 121)	$a = 5.070$	Hf 8i	0.75	0.75	0.375
		$b = 5.070$	O1 4c	0.0	0.5	0.0
		$c = 10.216$	O2 4e	0.0	0.0	0.25
			O3 4d	0.0	0.5	0.25
			O4 2a	0.0	0.0	0.0

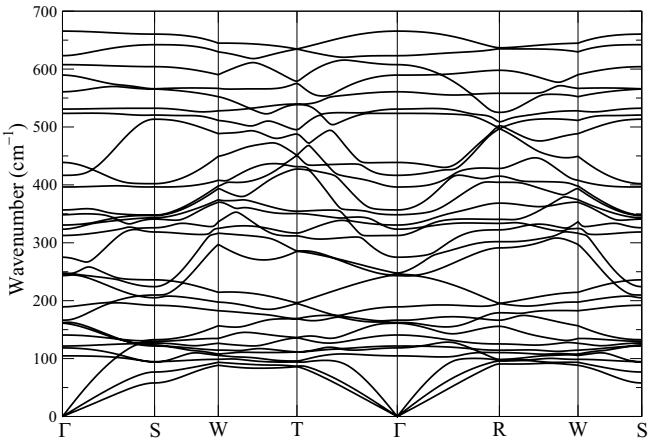

FIG. 5. Calculated phonon spectrum of the low-energy *Ibam*-Hf_2O_3 structure with ordered vacancies revealing its dynamical stability.

We conjecture that, during the electroforming process, *Ibam*-Hf_2O_3 is likely formed in the filaments, offering the stable frame, which allows for oxygen migration through the one-dimensional channels inherent to its structure. Filling up the channels with oxygen would then lead to the "off" state, i.e., Hf_4O_7 phase, whose narrow band gap can explain the significantly lower resistivity of the electroformed material in comparison to the host HfO_2. In the "on" state, oxygen anions migrate out of the channels; if a metallic Hf electrode is used, according to our analysis of region (*i*), it acts as a natural reservoir for the anions arriving from the oxide region. In order to provide an additional checkpoint for this hypothesis, we have calculated the energy barrier for oxygen migration through the one-dimensional channels of *Ibam*-Hf_2O_3, which amounts to 0.51 eV (see Table III). This barrier is significantly lower than both that for the migration of a neutral oxygen vacancy in the monoclinic HfO_2 (∼2.5 eV) [58] and even that of a positively charged vacancy (∼0.7 eV, Ref. [59]). Studying the structure of *Ibam*-Hf_2O_3 in detail (see Fig. 4) we find the need for one further check. Namely, the structural frame (i.e., the *Ibam*-Hf_2O_3 phase itself), which we assume provides the channels for oxygen migration, also contains oxygen. If this frame is to be rigid against a collapse in case its constitutive oxygen migrates out of it, the energy cost for this process needs to be significantly higher than the one of oxygen migrating through a channel. We therefore also calculated the barrier for an oxygen migrating out of the frame and into a channel, and find that it is indeed much higher, ∼1.73 eV. We therefore conclude that this is a valid hypothesis and investigate its further practical consequences.

Despite the fact that HfO_2 is well integrated in the semiconductor industry, applications of HfO_2 in commercial ReRAM devices are still limited, due to its unstable resistive switching behavior, although the conductive filaments formed by the electric-field induced oxygen vacancies were investigated extensively. One of the critical nonuniform parameters of resistive switching is the random conductive filament formation and rupture process. A large effort of experimental works is directed to finding ways of confining the conductive filament in the host oxide insulator, in order to improve the uniformity of resistive switching characteristics. It was found that, aside from embedding nanocrystals and multilayer structures, doping with foreign elements is an easy and effective way to improve resistive switching properties [60–62]. Therefore, in order to better understand the ionic conduction properties of the predicted *Ibam*-Hf_2O_3 phase, we calculated migration barriers for the most important elements, typically used for doping HfO_2 and as electrodes (see Table III). The barriers were calculated in a $2 \times 2 \times 2$ supercell of *Ibam*-Hf_2O_3 structure. Transition metal atoms were treated as nonmagnetic cations. As mentioned above, the migration barrier for oxygen (self)diffusion in *Ibam*-Hf_2O_3 is about 0.5 eV. The corresponding barrier for Hf atoms (self)diffusion along voids is found to be higher than for oxygen, indicating preferable role of oxygen vacancies in ion migration during switching processes. So far, this finding is in full agreement to the widely accepted mechanism of the resistive switching, with the dominant role of oxygen migration, supported experimentally [8]. Surprisingly, migration of cations with much bigger radii than that of oxygen, such as Os and Pt, was found to be even *easier* than for oxygen. Therefore, the role of these cations in resistive switching should be reconsidered (although, admittedly, it is unlikely that Pt would leave an electrode and get into the channels in the first place). Migration barriers for Zr, Ru, Zn, Cd, and Ag are higher than that for oxygen diffusion, but smaller than that of Hf. Finally, we found a set of "heavy to move" cations, Y and La, with migration barriers higher than 2 eV. Doping with these cations would block the ionic conductivity in HfO_x suboxides. This fact could be used for creating preferential sites for forming conductive filaments. This, in turn, should improve endurance of the device, as was observed in the case of nanotip confinement of geometric conductive filament in HfO_2-ReRAM [63].

IV. CONCLUSIONS

Using an evolutionary algorithm combined with *ab initio* calculations, we investigated the Hf-O composition diagram on the basis of about 5500 calculated (structural and chemical) configurations, and analyzed the crystal structures of metastable phases, focusing on their role in resistive switching. Aside from the energetically unlikely superoxide region, the obtained composition diagram revealed three distinct important regions:

TABLE III. Migration barriers (in eV) for important cations calculated for the *Ibam*-Hf_2O_3 phase with one-dimensional open channels.

O 0.51	Al 1.06							
Sc 0.93	Ti 0.94	V 1.37	Mn 1.21	Fe 0.62	Co 0.99	Ni 0.98	Cu 1.1	Zn 0.56
Y 2.29	Zr 0.59	Nb 1.42		Ru 0.52			Ag 0.68	Cd 0.49
La 2.81	Hf 0.72	Ta 0.76		Os 0.39		Pt 0.48		

(1) Metal-rich phases, based on the hexagonal close packed lattice of metallic Hf, where some of the octahedral voids are occupied by oxygen atoms. We find that the solubility of oxygen in metallic Hf is very high, indicating that Hf can be used as an active electrode which hosts oxygen atoms that migrate out of the oxide region during the switching.

(2) Region $1 \leqslant x \leqslant 1.25$. Intermediate phases of HfO_x with monoclinic structure.

(3) Region $1.5 \leqslant x \leqslant 1.75$. Suboxide phases with fluorite-like (pseudo)tetragonal structure.

In the latter two regions, all the structures with lowest formation energies are characterized by the common feature of periodic lattices of one-dimensional oxygen vacancy channels embedded in the respective monoclinic or tetragonal frame. The oxygen concentration determines the degree of oxygen filling of the channels, whereas channels that are either completely filled or empty are either insulating or metallic, respectively.

We investigated the migration barriers for metallic cations through the channels in the ordered *Ibam*-Hf_2O_3 phase and found that some cations, like Y, La, V, and Nb, have very large migration barriers and would block the ionic conductivity in the oxygen deficient phases.

Finally, we relate our findings obtained in a study dealing with crystalline phases at the microscopic level to the broader picture of a macroscopic sample (a ReRAM device) with localized filaments of diameters between approximately 5 and 20 nm. Our results suggest that during the nonequilibrium process of filament formation and depending on the oxygen concentration there is a great tendency of the formation of meta-stable nanophases of the type discussed in O-deficient hafnia regions with one-dimensional vacancy channels. Although the boundary of the nanophase to the HfO_2 host cannot be fully neglected, the existence of such one-dimensional conductance channels is supported by a recent experiment [64] where a conductance quantization in $Pt/HfO_x/TiN$ structures was observed.

The ReRAM devices based on hafnia with metastable nanophases containing one-dimensional vacancy channels may operate over a wide range of oxygen concentrations involving the monoclinic as well as the fluorite-like suboxide phase, separated in the phase diagram by a gap in the range of oxygen concentrations, where no phases with low formation energy exist. Therefore, a well controlled content of oxygen in "set" and "reset" guarantees operations within the same structural frame and minimizes the mechanical degradation of the crystal structure during the switching processes, thus increasing the endurance of the ReRAM devices.

Care has to be taken when using electrodes of difficultly migrating cations, as ions may diffuse from the electrode into the channels of the formed filament, which could impair or possibly completely destroy the functionality of the memory cell. On the other hand, controlled doping of hafnia with such cations could possibly be used in order to increase the information density of memory cells by predetermining the position of the conductive filaments in a "controlled" forming process.

Our results invite experimental efforts to structurally analyze filaments in HfO_2 with respect to channel-like nanophases. This is a challenging problem as the open channels likely contain different amounts of randomly distributed oxygen. We further suggest the dedicated growth of specific metastable phases as single crystals, with the purpose to attain a better understanding of the ionic migration through these structures with open channels, of the electrode behavior in the switching process, and of the role of dopants. On the basis of such a systematic knowledge, more reliable devices with a high information density high endurance and retention could be engineered. We note that the major trends found here for HfO_2 are also valid for ZrO_2 and partly in Y_2O_3 [65].

ACKNOWLEDGMENTS

We gratefully acknowledge the financial support by Deutsche Forschungsgemeinschaft (DFG) through SFB 917 "Nanoswitches", as well as the support of the Jülich Supercomputing Centre (JSC) (project jiff38) and the JARA-HPC Partition (project jara0126) in acquiring computing resources. We are grateful to Prof. Dr. Roger A. De Souza and Dr. Gustav Bihlmayer for invaluable discussions.

[1] J. S. Lee, S. Lee, and T. W. Noh, Appl. Phys. Rev. **2**, 031303 (2015).

[2] R. Waser and M. Aono, Nat. Mater. **6**, 833 (2007).

[3] G. Bersuker, D. C. Gilmer, D. Veksler, P. Kirsch, L. Vandelli, A. Padovani, L. Larcher, K. McKenna, A. Shluger, V. Iglesias *et al.*, J. Appl. Phys. **110**, 124518 (2011).

[4] A. Wedig, M. Luebben, D.-Y. Cho, M. Moors, K. Skaja, V. Rana, T. Hasegawa, K. K. Adepalli, B. Yildiz, R. Waser *et al.*, Nat. Nano **11**, 67 (2016).

[5] D.-Y. Cho, M. Luebben, S. Wiefels, K.-S. Lee, and I. Valov, ACS Appl. Mater. Interfaces **9**, 19287 (2017).

[6] T. Hantschel, C. Demeulemeester, P. Eyben, V. Schulz, O. Richard, H. Bender, and W. Vandervorst, Phys. Status Solidi A **206**, 2077 (2009).

[7] U. Celano, J. Op de Beeck, S. Clima, M. Luebben, P. M. Koenraad, L. Goux, I. Valov, and W. Vandervorst, ACS Appl. Mater. Interfaces **9**, 10820 (2017).

[8] L. Goux, P. Czarnecki, Y. Y. Chen, L. Pantisano, X. P. Wang, R. Degraeve, B. Govoreanu, M. Jurczak, D. J. Wouters, and L. Altimime, Appl. Phys. Lett. **97**, 243509 (2010).

[9] S. Kumar, Z. Wang, X. Huang, N. Kumari, N. Davila, J. P. Strachan, D. Vine, A. L. D. Kilcoyne, Y. Nishi, and R. S. Williams, Appl. Phys. Lett. **110**, 103503 (2017).

[10] K.-L. Lin, T.-H. Hou, J. Shieh, J.-H. Lin, C.-T. Chou, and Y.-J. Lee, J. Appl. Phys. **109**, 084104 (2011).

[11] B. Magyari-Köpe, S. G. Park, H.-D. Lee, and Y. Nishi, J. Mater. Sci. **47**, 7498 (2012).

[12] S. G. Park, B. Magyari-Köpe, and Y. Nishi, IEEE Electron Device Lett. **32**, 197 (2011).

[13] K. Szot, W. Speier, G. Bihlmayer, and R. Waser, Nat. Mater. **5**, 312 (2006).

[14] M. Rogala, G. Bihlmayer, W. Speier, Z. Klusek, C. Rodenbücher, and K. Szot, Adv. Funct. Mater. **25**, 6382 (2015).

[15] C. Lenser, A. Koehl, I. Slipukhina, H. Du, M. Patt, V. Feyer, C. M. Schneider, M. Lezaic, R. Waser, and R. Dittmann, Adv. Funct. Mater. **25**, 6360 (2015).

[16] I. Slipukhina and M. Ležaić, Phys. Rev. B **90**, 155133 (2014).

[17] D.-H. Kwon, K. M. Kim, J. H. Jang, J. M. Jeon, M. H. Lee, G. H. Kim, X.-S. Li, G.-S. Park, B. Lee, S. Han *et al.*, Nat. Nanotechnol. **5**, 148 (2010).

[18] R. F. Bartholomew and D. R. Frankl, Phys. Rev. **187**, 828 (1969).

[19] S. Andersson, B. Collén, U. Kuylenstierna, and A. Magnéli, Acta Chem. Scand. **11**, 1641 (1957).

[20] C. Tang, D. Zhou, and Q. Zhang, Mater. Lett. **79**, 42 (2012).

[21] C. Hauf, R. Kniep, and G. Pfaff, J. Mater. Sci. **34**, 1287 (1999).

[22] B. Naoufal and L. Damien, Chem. Vap. Deposition **20**, 299 (2014).

[23] N. S. H. Gunda, B. Puchala, and A. Van der Ven, Phys. Rev. Materials **2**, 033604 (2018).

[24] K. Kamiya, M. Y. Yang, T. Nagata, S.-G. Park, B. Magyari-Köpe, T. Chikyow, K. Yamada, M. Niwa, Y. Nishi, and K. Shiraishi, Phys. Rev. B **87**, 155201 (2013).

[25] S. M. Aspera, H. Kasai, H. Kishi, N. Awaya, S. Ohnishi, and Y. Tamai, J. Electron. Mater. **42**, 143 (2013).

[26] K.-H. Xue and X.-S. Miao, J. Appl. Phys. **123**, 161505 (2018).

[27] K. P. McKenna, Modell. Simul. Mater. Sci. Eng. **22**, 025001 (2014).

[28] K.-H. Xue, P. Blaise, L. R. C. Fonseca, G. Molas, E. Vianello, B. Traoré, B. D. Salvo, G. Ghibaudo, and Y. Nishi, Appl. Phys. Lett. **102**, 201908 (2013).

[29] M. Lanza, K. Zhang, M. Porti, M. Nafría, Z. Y. Shen, L. F. Liu, J. F. Kang, D. Gilmer, and G. Bersuker, Appl. Phys. Lett. **100**, 123508 (2012).

[30] B. P. Burton and A. van de Walle, Calphad **37**, 151 (2012).

[31] J. Zhang, A. R. Oganov, X. Li, K.-H. Xue, Z. Wang, and H. Dong, Phys. Rev. B **92**, 184104 (2015).

[32] A. R. Oganov and C. W. Glass, J. Chem. Phys. **124**, 244704 (2006).

[33] A. R. Oganov, A. O. Lyakhov, and M. Valle, Acc. Chem. Res. **44**, 227 (2011).

[34] A. O. Lyakhov, A. R. Oganov, H. T. Stokes, and Q. Zhu, Comput. Phys. Commun. **184**, 1172 (2013).

[35] K.-H. Xue, P. Blaise, L. R. C. Fonseca, and Y. Nishi, Phys. Rev. Lett. **110**, 065502 (2013).

[36] J. P. Perdew, K. Burke, and M. Ernzerhof, Phys. Rev. Lett. **77**, 3865 (1996).

[37] V. I. Anisimov, F. Aryasetiawan, and A. I. Lichtenstein, J. Phys.: Condens. Matter **9**, 767 (1997).

[38] A. R. Oganov, Y. Ma, A. O. Lyakhov, M. Valle, and C. Gatti, Rev. Mineral. Geochem. **71**, 271 (2010).

[39] R. Martoňák, A. Laio, and M. Parrinello, Phys. Rev. Lett. **90**, 075503 (2003).

[40] G. Kresse and J. Hafner, Phys. Rev. B **47**, 558 (1993).

[41] G. Kresse and J. Furthmüller, Phys. Rev. B **54**, 11169 (1996).

[42] G. Kresse and D. Joubert, Phys. Rev. B **59**, 1758 (1999).

[43] P. E. Blöchl, Phys. Rev. B **50**, 17953 (1994).

[44] G. I. Csonka, J. P. Perdew, A. Ruzsinszky, P. H. T. Philipsen, S. Lebègue, J. Paier, O. A. Vydrov, and J. G. Ángyán, Phys. Rev. B **79**, 155107 (2009).

[45] A. Hanke, K. Z. Rushchanskii, C. Friedrich, S. Blügel, and M. Ležaić (unpublished).

[46] D. Alfè, Comput. Phys. Commun. **180**, 2622 (2009).

[47] G. Henkelman, B. P. Uberuaga, and H. Jónsson, J. Chem. Phys. **113**, 9901 (2000).

[48] V. Miikkulainen, M. Leskelä, M. Ritala, and R. L. Puurunen, J. Appl. Phys. **113**, 021301 (2013).

[49] M. Hirabayashi, S. Yamaguchi, and T. Arai, J. Phys. Soc. Jpn. **35**, 473 (1973).

[50] V. V. Afanas'ev, A. Stesmans, L. Pantisano, S. Cimino, C. Adelmann, L. Goux, Y. Y. Chen, J. A. Kittl, D. Wouters, and M. Jurczak, Appl. Phys. Lett. **98**, 132901 (2011).

[51] X. Zhong, I. Rungger, P. Zapol, H. Nakamura, Y. Asai, and O. Heinonen, Phys. Chem. Chem. Phys. **18**, 7502 (2016).

[52] S. U. Sharath, T. Bertaud, J. Kurian, E. Hildebrandt, C. Walczyk, P. Calka, P. Zaumseil, M. Sowinska, D. Walczyk, A. Gloskovskii *et al.*, Appl. Phys. Lett. **104**, 063502 (2014).

[53] J. P. Perdew and A. Zunger, Phys. Rev. B **23**, 5048 (1981).

[54] A. D. Becke, J. Chem. Phys. **98**, 5648 (1993).

[55] P. J. Stephens, F. J. Devlin, C. F. Chabalowski, and M. J. Frisch, J. Phys. Chem. **98**, 11623 (1994).

[56] J. Heyd, G. E. Scuseria, and M. Ernzerhof, J. Chem. Phys. **118**, 8207 (2003).

[57] J. Heyd, G. E. Scuseria, and M. Ernzerhof, J. Chem. Phys. **124**, 219906 (2006).

[58] Y. Dai, Z. Pan, F. Wang, and X. Li, AIP Adv. **6**, 085209 (2016).

[59] K. McKenna and A. Shluger, Appl. Phys. Lett. **95**, 222111 (2009).

[60] Y. S. Chen, B. Chen, B. Gao, L. F. Liu, X. Y. Liu, and J. F. Kang, J. Appl. Phys. **113**, 164507 (2013).

[61] C.-S. Peng, W.-Y. Chang, Y.-H. Lee, M.-H. Lin, F. Chen, and M.-J. Tsai, Electrochem. Solid-State Lett. **15**, H88 (2012).

[62] D. Duncan, B. Magyari-Köpe, and Y. Nishi, Phys. Rev. Appl. **7**, 034020 (2017).

[63] G. Niu, P. Calka, M. Auf der Maur, F. Santoni, S. Guha, M. Fraschke, P. Hamoumou, B. Gautier, E. Perez, C. Walczyk *et al.*, Sci. Rep. **6**, 25757 (2016).

[64] S. U. Sharath, S. Vogel, L. Molina-Luna, E. Hildebrandt, C. Wenger, J. Kurian, M. Duerrschnabel, T. Niermann, G. Niu, P. Calka *et al.*, Adv. Funct. Mater. **27**, 1700432 (2017).

[65] K. Z. Rushchanskii, S. Blügel, and M. Ležaić, Faraday Discuss. (2019), doi:10.1039/C8FD00104A.